GEOPHYSICS, VOL. 55, NO. 9 (SEPTEMBER 1990); P. 1223–1234, 19 FIGS.

DOI:10.1190/1.1442938

Angle–dependent reflectivity by means of prestack migration

C. G. M. de Bruin*, C. P. A. Wapenaar*, and A. J. Berkhout*

ABSTRACT

Most present day seismic migration schemes determine only the zero–offset reflection coefficient for each grid point (depth point) in the subsurface. In matrix notation, the zero–offset reflection coefficient is found on the diagonal of a reflectivity matrix operator that transforms the illuminating source–wave field into a reflected–wave field. However, angle dependent reflectivity information is contained in the full reflectivity matrix.

Our objective is to obtain angle–dependent reflection coefficients from seismic data by means of prestack migration (multisource, multioffset). After downward extrapolation of source and reflected wave fields to one depth level, the rows of the reflectivity matrix (representing angle–dependent reflectivity information for each grid point at that depth level) are recovered by deconvolving the reflected wave fields with the related source wave fields.

This process is carried out in the space–frequency domain. In order to preserve the angle–dependent reflectivity in the imaging we must not only add all frequency contributions but we should extend the imaging principle by adding along lines of constant angle in the wavenumber–frequency domain. This procedure is carried out for each grid point. The resulting amplitude information provides a rigorous approach to amplitude-versus-offset related methods.

The new imaging technique has been tested on media with horizontal layers. However, with our shot–record oriented algorithm it is possible to handle any subsurface geometry. The first tests show excellent results up to high angles, both in the acoustic and in the elastic case. With angle–dependent reflectivity information it becomes feasible to derive detailed velocity and density information in a subsequent stratigraphic inversion step.

INTRODUCTION

Advanced seismic inversion techniques are designed to extract structural and lithological information from seismic surface data. One of these techniques is seismic migration, which images the structure of the subsurface in terms of its reflectivity. This paper is a first step toward a more refined prestack–migration technique, which takes into account the angle–dependent properties of the reflectivity.

According to Berkhout (1985), the physical model for one–way wave propagation can be simply represented in terms of matrix multiplications using a downward propagation matrix, a reflectivity matrix, and an upward propagation matrix. The reflectivity properties of a reflector are described by reflectivity matrix $\underline{\mathbf{R}}$. In seismic migration it is common practice to represent reflectivity by a single reflection coefficient per depth point (Claerbout, 1976). In this case the reflectivity matrix would be a diagonal matrix, each diagonal element representing the zero–offset reflection coefficient at a lateral position at a constant depth level: $R(x, z_i)$ in the two-dimensional (2–D) case. Only information about the detailed acoustic impedance can be retrieved from this zero–offset reflection coefficient.

This paper attempts extraction of more information from the seismic data than just the zero–offset reflectivity. This information will be in the form of space–variant, angle–dependent reflectivity information at each grid point: $R(x, z_i; \alpha)$ in the 2–D case. With this additional information the detailed medium parameters (ρ, c_p, c_s) can be determined. The retrieval of angle–dependent reflectivity from seismic data is based on shot–record migration in the space–frequency (x, ω) domain as proposed by Berkhout (1985). In contrast with conventional amplitude versus offset techniques (AVO), complicated subsurfaces can be handled.

Presented at the 58th Society of Exploration Geophysicists Annual Meeting. Manuscript received by the Editor July 17, 1989; revised manuscript received March 5, 1990.
*Delft University of Technology, Laboratory of Seismics and Acoustics, P.O. Box 5046, 2600 GA Delft, The Netherlands.

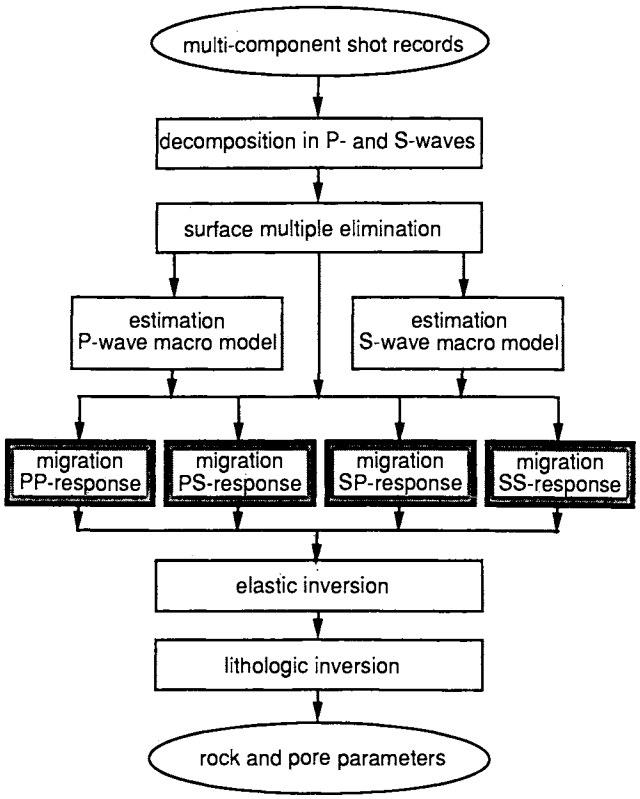

FIG. 1. Elastic seismic processing scheme. The highlighted part of the scheme is the subject discussed in this paper.

Resnick et al. (1987) discuss the fact that dips introduce serious problems for AVO analysis. They conclude that performing prestack migration on the data before doing AVO analysis is a necessity. In this paper the prestack migration itself yields angle-dependent reflectivity directly from the surface data.

The method described in this paper forms part of the Delft approach to the inversion of elastic data (Berkhout and Wapenaar, 1988). It involves the following steps (Figure 1):

Decomposition of the multicomponent seismic data into *P*- and *S*-wave responses (Herrmann et al., 1989);

Elimination of surface related multiples and conversions (Verschuur et al., 1989);

Macromodel estimation (*P*- and *S*-wave velocities) (Cox et al., 1989);

Prestack migration, yielding angle-dependent *P-P*, *S-P*, *P-S*, and *S-S* reflectivity (this paper);

Elastic inversion, yielding the detailed medium parameters (ρ, c_p, c_s) (De Haas and Berkhout, 1989);

Lithologic inversion, yielding rock and pore parameters (Lörtzer and Berkhout, 1989).

This step-wise approach is a powerful alternative to linear and nonlinear inversion schemes, as proposed for instance by Tarantola (1986), which aim at resolving the detailed medium parameters directly from the (multicomponent) seismic data.

THE FORWARD MODEL

Following Berkhout (1985), the monochromatic acoustic two-dimensional (2-D) forward model of a seismic shot record can be written as follows (in matrix notation):

$$\mathbf{P}^-(z_0) = \left[\sum_i \underline{\mathbf{W}}^-(z_0, z_i)\underline{\mathbf{R}}(z_i)\underline{\mathbf{W}}^+(z_i, z_0)\right]\mathbf{S}^+(z_0). \quad (1)$$

Here $\mathbf{S}^+(z_0)$ describes one frequency component of the downgoing source wave field at z_0. Vector $\mathbf{P}^-(z_0)$ represents one frequency component of the acoustic pressure of all upgoing reflected wave fields, arriving back at the surface z_0. Matrices $\underline{\mathbf{W}}^+(z_i, z_0)$ and $\underline{\mathbf{W}}^-(z_0, z_i)$ describe the propagation of the downgoing source wave field and the upgoing reflected wave fields, respectively. A schematic illustration of this equation is shown in Figure 2. It contains the essentials of any echo acoustic technique: illumination, reflection, back propagation and detection. Wapenaar and Berkhout (1989) show that a similar forward model is valid for elastic three-dimensional (3-D) multicomponent seismic data *after* decomposition and surface multiple elimination. We will come back to this in one of the examples. For the moment, however, we restrict ourselves to the 2-D acoustic situation.

Reflectivity matrix $\underline{\mathbf{R}}(z_i)$ defines the relationship between the downward and upward traveling wave fields at z_i. The determination of matrix $\underline{\mathbf{R}}$ is generally complicated for a given subsurface model. Therefore, often $\underline{\mathbf{R}}$ is taken as a diagonal matrix. The inhomogeneities at z_i are thus considered to be "locally reacting," i.e., one point of the incident wave field contributes to one point of the reflected wave field at the same lateral position. Note that in this case the rows of $\underline{\mathbf{R}}(z_i)$ contain only one nonzero sample.

Ideally, one sample of the reflected wave field $P^-(x_j, z_i, \omega)$ at the reflector is defined as a spatially weighted average of the total incident wave field $S^+(x, z_i, \omega)$ at the reflector, according to

$$P^-(x_j, z_i, \omega) = \int_{-\infty}^{\infty} R_j(x_j - x, z_i, \omega)S^+(x, z_i, \omega)\, dx, \quad (2a)$$

or, in discretized form,

$$P^-(x_j, z_i, \omega) = \sum_m R_j(x_j - x_m, z_i, \omega)S^+(x_m, z_i, \omega)\Delta x, \quad (2b)$$

(where Δx is the lateral sampling interval), or, in matrix notation,

$$\mathbf{P}^-(z_i) = \underline{\mathbf{R}}(z_i)\mathbf{S}^+(z_i). \quad (2c)$$

(Figure 3). Here the mth element of vector $\mathbf{S}^+(z_i)$ contains $S^+(x_m, z_i, \omega)$, the mth element of the jth row of $\underline{\mathbf{R}}(z_i)$ contains $\Delta x R_j(x_j - x_m, z_i, \omega)$ and, finally, the jth element of vector $\mathbf{P}^-(z_i)$ contains $P^-(x_j, z_i, \omega)$. Equations (2a), (2b), and (2c) represent a generalized spatial convolution. Note that for a laterally invariant reflector we may replace equation (2a) by

$$P^-(x, z_i, \omega) = \int_{-\infty}^{\infty} R(x - x', z_i, \omega)S^+(x', z_i, \omega)\, dx', \quad (3a)$$

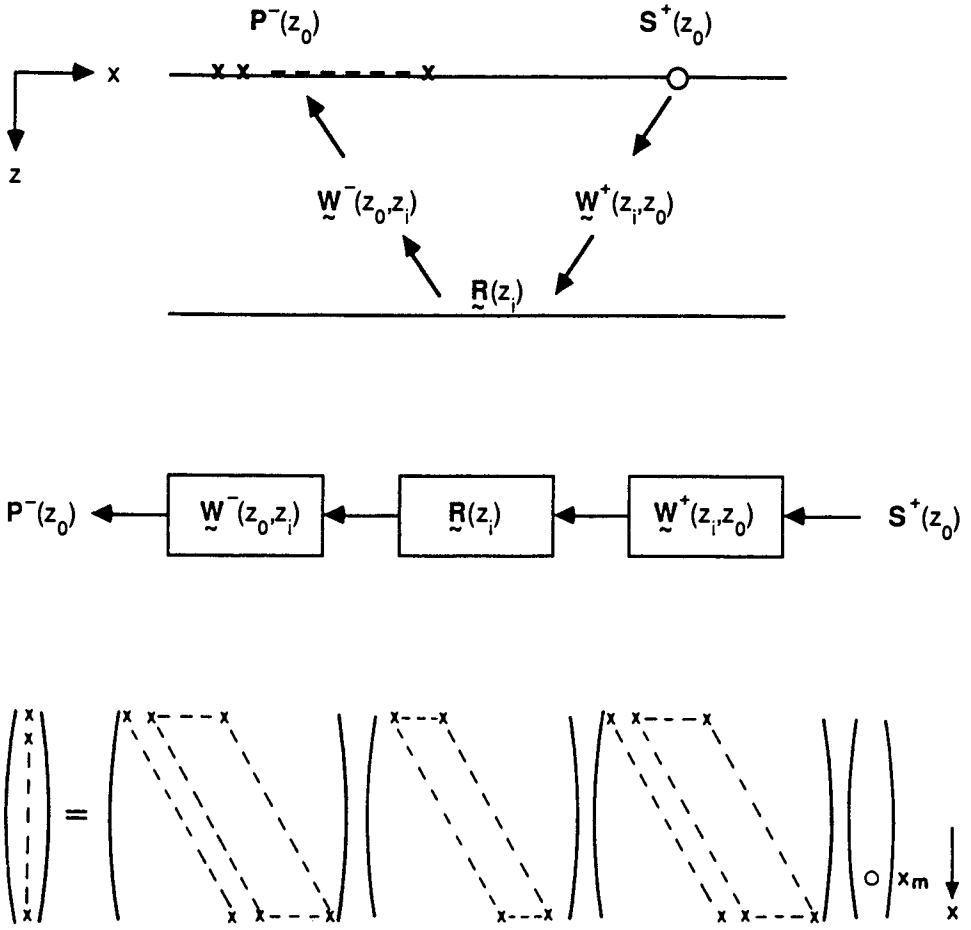

FIG. 2. Forward model of a seismic shot record after decomposition and surface multiple elimination in terms of matrix multiplications (no field patterns). The reflectivity matrix $\underset{\sim}{\mathbf{R}}$ transforms the downgoing wave field partially into an upgoing reflected wave field.

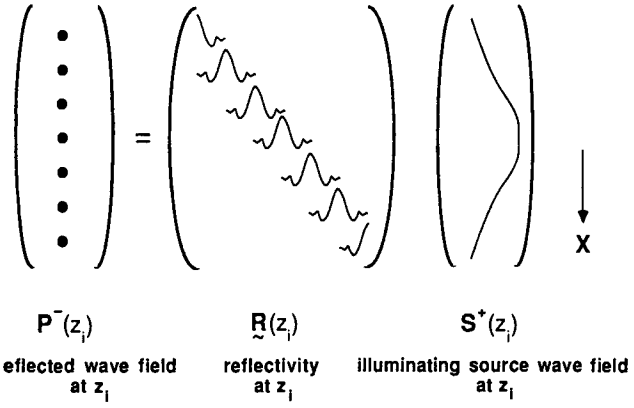

FIG. 3. Each row of the reflectivity matrix $\underset{\sim}{\mathbf{R}}$ represents a reflectivity convolution operator.

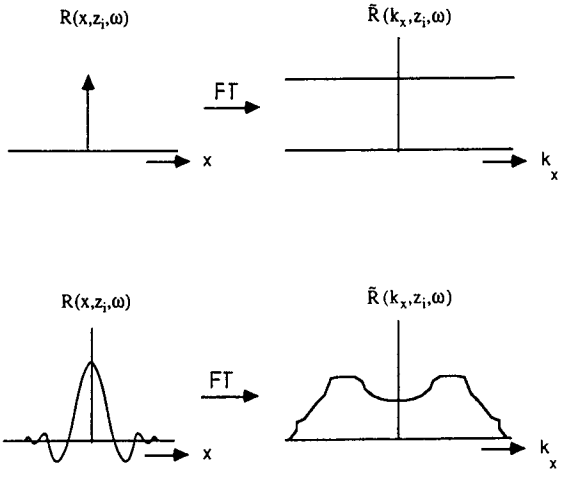

FIG. 4. (a) A locally reacting reflectivity operator (one row of matrix $\underset{\sim}{\mathbf{R}}$) corresponds to an *angle-independent* reflection function. (b) A non-locally reacting reflectivity operator corresponds to an angle-dependent reflection function.

or, symbolically,

$$P^-(x, z_i, \omega) = R(x, z_i, \omega) * S^+(x, z_i, \omega), \quad (3b)$$

where the asterisk denotes a conventional spatial convolution along the x-axis. In the following we refer to the rows of matrix $\underline{\mathbf{R}}(z_i)$ as (generalized) reflectivity convolution operators. A reflectivity convolution operator defines angle-dependent reflection as follows. We apply a spatial Fourier transform to equation (3b), yielding

$$\tilde{P}^-(k_x, z_i, \omega) = \tilde{R}(k_x, z_i, \omega)\tilde{S}^+(k_x, z_i, \omega), \quad (4)$$

where the tilde denotes the wavenumber (k_x) domain. In order to obtain an expression for $\tilde{R}(k_x, z_i, \omega)$, we start with the well-known angle-dependent reflection coefficient $R(z_i; \alpha)$ for two acoustic half-spaces separated by an interface at z_i:

$$R(z_i; \alpha) = \frac{\rho_2 c_2 \cos\alpha - \rho_1\sqrt{c_1^2 - c_2^2\sin^2\alpha}}{\rho_2 c_2 \cos\alpha + \rho_1\sqrt{c_1^2 - c_2^2\sin^2\alpha}}. \quad (5)$$

c_1 and c_2 are the velocities, ρ_1 and ρ_2 are the mass densities of the upper and lower half-space, respectively, and α is the angle of incidence. By substituting $k_1 = \omega/c_1$, $k_2 = \omega/c_2$, and $k_x = k_1 \sin\alpha$ in equation (5) we obtain

$$\tilde{R}(k_x, z_i, \omega) = \frac{\rho_2\sqrt{k_1^2 - k_x^2} - \rho_1\sqrt{k_2^2 - k_x^2}}{\rho_2\sqrt{k_1^2 - k_x^2} + \rho_1\sqrt{k_2^2 - k_x^2}}. \quad (6)$$

$\tilde{R}(k_x, z_i, \omega)$ is named the (angle-dependent) reflection function at level z_i. Note that $\tilde{R}(k_x, z_i, \omega)$ is frequency-dependent as opposed to $R(z_i; \alpha)$.

If a reflector is locally reacting, then $\underline{\mathbf{R}}$ is a diagonal matrix. Hence, for a laterally invariant, locally reacting reflector we may write $R(x, z_i, \omega) = R_0(z_i)\delta(x)$ or $\tilde{R}(k_x, z_i, \omega) = R_0(z_i)$, so the reflection function does not vary with the angle of incidence. An example of a locally reacting reflector is an interface between two homogeneous liquids which have a density contrast only (Figure 4a). In this case $\rho_1 \neq \rho_2$, $c_1 = c_2$ in equation (5) and the reflection coefficient $R(z_i; \alpha)$ becomes

$$R(z_i; \alpha) = R_0(z_i) = \frac{\rho_2 - \rho_1}{\rho_2 + \rho_1}. \quad (7)$$

The locally reacting assumption is equivalent to assuming *angle-independent* reflectivity.

The assumption of angle-independent reflectivity in the general practice of seismic migration is only justified in the situation of small emergence angles (and in the case just described). For larger angles, however, the locally reacting assumption is no longer justified and angle-dependent reflectivity must be considered. In this case matrix $\underline{\mathbf{R}}$ will have a band structure and the reflection function will show angle dependency, as seen in Figure 4b. Therefore prestack migration should ideally resolve the full matrix $\underline{\mathbf{R}}$ rather than just the diagonal elements.

PRESTACK MIGRATION

The forward model for one seismic experiment, formulated in equation (1), can be rewritten into

$$\mathbf{P}^-(z_0) = \underline{\mathbf{X}}(z_0)\mathbf{S}^+(z_0), \quad (8a)$$

with

$$\underline{\mathbf{X}}(z_0) = \sum_i [\underline{\mathbf{W}}^-(z_0, z_i)\underline{\mathbf{R}}(z_i)\underline{\mathbf{W}}^+(z_i, z_0)]. \quad (8b)$$

In equation (8a) $\mathbf{P}^-(z_0)$ represents one monochromatic shot record and $\underline{\mathbf{X}}(z_0)$ describes the medium response. In the inverse problem we have to determine $\underline{\mathbf{R}}$, assuming that the seismic measurements $\mathbf{P}^-(z_0)$, the source wave field $\mathbf{S}^+(z_0)$, and the macrosubsurface model are given.

The inversion process consists of a number of steps. First, one determines $\underline{\mathbf{X}}(z_0)$ by inverting equation (8a) for all available shot records (deconvolution). The next step is a compensation for propagation effects in $\underline{\mathbf{X}}(z_0)$ for each separate depth level. Assuming a lossless medium, the propagation effects between the surface and depth level z_k can be eliminated by

$$\underline{\mathbf{X}}(z_k) = \underline{\mathbf{F}}^-(z_k, z_0)\underline{\mathbf{X}}(z_0)\underline{\mathbf{F}}^+(z_0, z_k), \quad (9a)$$

with

$$\underline{\mathbf{F}}^-(z_k, z_0) \triangleq [\underline{\mathbf{W}}^-(z_0, z_k)]^{-1} \approx [\underline{\mathbf{W}}^+(z_k, z_0)]^*, \quad (9b)$$

and

$$\underline{\mathbf{F}}^+(z_0, z_k) \triangleq [\underline{\mathbf{W}}^+(z_k, z_0)]^{-1} \approx [\underline{\mathbf{W}}^-(z_0, z_k)]^*. \quad (9c)$$

(see Berkhout, 1985). For implementation, the reader is referred to Kinneging et al. (1989). The final step is imaging. Rewrite equation (9a) by substituting equation (8b), yielding

$$\underline{\mathbf{X}}(z_k) = \underline{\mathbf{R}}(z_k) + \sum_{i \neq k} [\underline{\mathbf{F}}^-(z_k, z_0)\underline{\mathbf{W}}^-(z_0, z_i) \times \underline{\mathbf{R}}(z_i)\underline{\mathbf{W}}^+(z_i, z_0)\underline{\mathbf{F}}^+(z_0, z_k)]. \quad (10)$$

Conventional imaging involves

$$\langle\underline{\mathbf{R}}(z_k)\rangle = \frac{\Delta\omega}{2\pi}\sum_\omega \underline{\mathbf{X}}(z_k), \quad (11)$$

where only the diagonal elements of $\langle\underline{\mathbf{R}}(z_k)\rangle$ are selected. (Keep in mind that summing over all frequency components is equivalent to inverse Fourier transforming and selecting the zero-time component.) These diagonal elements represent the average reflectivity at depth level z_k. Our aim, however, is to resolve angle-dependent reflectivity from the full reflectivity matrix.

OBTAINING ANGLE-DEPENDENT REFLECTIVITY

In the practice of seismic migration, only the diagonal elements of matrix $\underline{\mathbf{R}}(z_k)$ used to be resolved. As argued in a previous section, to obtain angle-dependent reflectivity information the full matrix $\underline{\mathbf{R}}(z_k)$ has to be computed. In the following we restrict ourselves to interpreting the jth row of the reflectivity matrix $\underline{\mathbf{R}}(z_k)$ [see also equation (2)]. This is the reflectivity convolution operator $R_j(x_j - x, z_k, \omega)$. The spatial Fourier transform of $R_j(x, z_k, \omega)$ defines the angle-dependent reflection function $\tilde{R}_j(k_x, z_k, \omega)$ for depth point (x_j, z_k). In the broad-band case the imaging step must be taken into account. Therefore another imaging operator will be defined based on the fact that the reflection functions

must be summed along lines of constant angle in the $k_x - \omega$ domain, that is, along lines of constant ray parameter

$$\frac{k_x}{\omega} = \frac{\sin \alpha}{c} = \frac{1}{c_x}. \tag{12}$$

In the seismic literature, c_x^{-1} is generally referred to as the ray parameter p (horizontal slowness). If we replace the wavenumber variable k_x by the ray parameter $p = k_x/\omega$, according to

$$\tilde{X}_j(k_x, z_k, \omega) \rightarrow \tilde{X}_j(p, z_k, \omega), \tag{13}$$

("mapping"), then imaging can be carried out in the $p - \omega$ domain along lines of constant p. This yields a true amplitude estimate of the angle-dependent reflectivity:

$$\langle \tilde{R}_j(p, z_k) \rangle = \frac{1}{N_\omega} \sum_\omega \tilde{X}_j(p, z_k, \omega). \tag{14}$$

N_ω is a correction for the frequency content of the wavelet. For example, for a box-shaped frequency spectrum N_ω is equal to the number of frequency components. The whole procedure is repeated for each extrapolation depth level, yielding a $p - z$ panel for each lateral position.

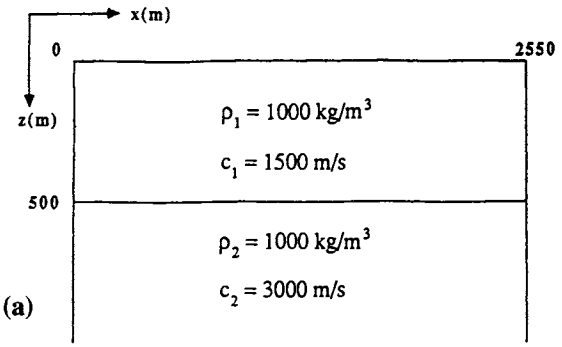

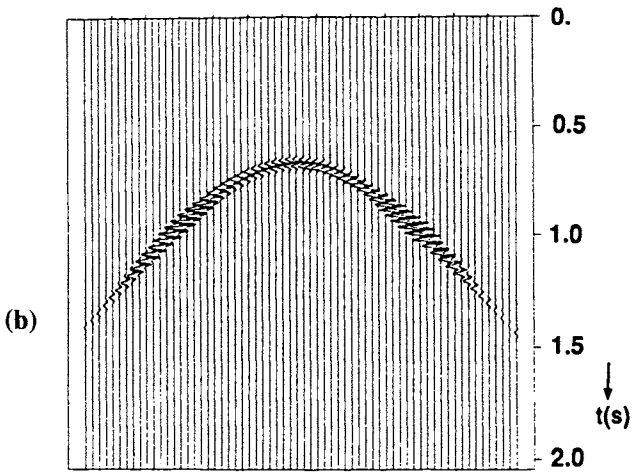

FIG. 5. (a) Subsurface model of a horizontally layered acoustic medium, containing one reflector at depth $z_1 = 500$ m. (b) Simulated seismic response from the acoustic model.

Example

As an illustration, consider a simple acoustic subsurface model (Figure 5a). Figure 5b displays the simulated seismic response of one shot record. The seismic data were modeled with an acoustic two-way modeling scheme which automat-

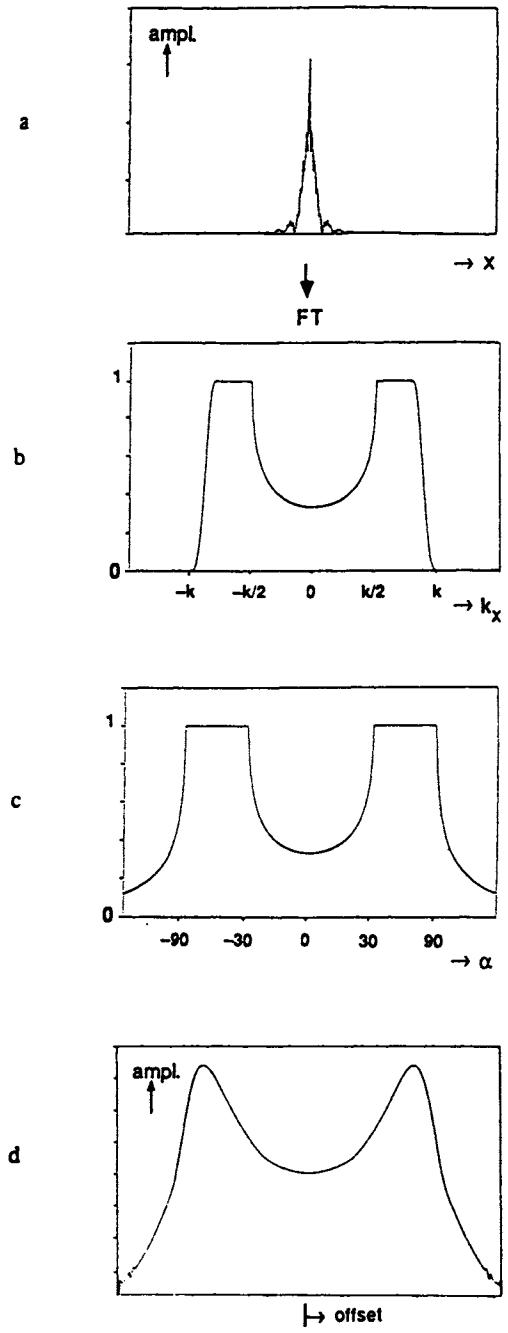

FIG. 6. (a) Modulus of the convolution operator $R_{128}(x, z_1 = 500$ m, $f = 50$ Hz). (b) Modulus of the angle-dependent reflection function $\tilde{R}_{128}(k_x, z_1 = 500$ m, $f = 50$ Hz), obtained by spatially Fourier transforming the (complex) convolution operator in (a). (c) Exact angle-dependent reflection coefficient $R(z_i; \alpha)$. Keep in mind that $k_x = (2\pi f/c_1) \sin \alpha$. (d) AVO result, obtained via amplitude picking along the hyperbola of Figure 5b.

ically incorporates the angle dependent reflectivity. First we show for frequency $f = 50$ Hz how the (monochromatic) angle-dependent reflection function $\tilde{R}_j(k_x, z_1 = 500\text{ m}, f = 50$ Hz) at $x_j = 1280$ m ($j = 128$, $\Delta x = 10$ m) is retrieved from the (simulated) surface data.

After downward extrapolation to $z_1 = 500$ m, as described by equation (9a), the jth row of $\underset{\sim}{\mathbf{X}}(z_1)$ represents the reflectivity convolution operator $R_j(x_j - x, z_1 = 500\text{ m}, f = 50$ Hz), [keep in mind that for this simple model $\underset{\sim}{\mathbf{X}}(z_1) = \underset{\sim}{\mathbf{R}}(z_1)$, see equation (10)]. The modulus of $R_j(x, z_1 = 500\text{ m}, f = 50$ Hz) for $j = 128$, which contains the angle-dependent reflectivity information at reflector point ($x_{128} = 1280$ m, $z_1 = 500$ m), is plotted in Figure 6a. The peak in the middle of this operator is the zero-offset reflection coefficient that would be obtained with conventional prestack migration algorithms.

When we compute the spatial Fourier transform ($x \rightarrow k_x$) of this operator, we obtain the reflection function $\tilde{R}_j(k_x, z_1 = 500\text{ m}, f = 50$ Hz). The modulus of the complex monochro-

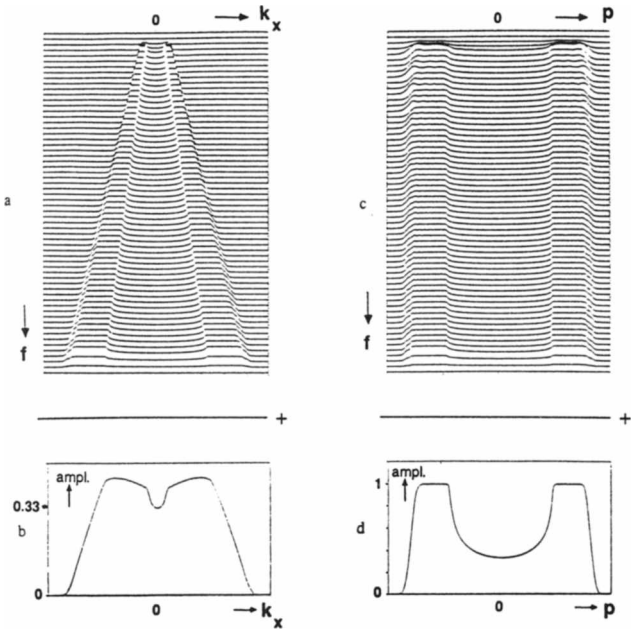

FIG. 7. Mapping from k_x to p and imaging, according to equations (13) and (14), respectively. (a) Modulus of the reflection function for different frequencies (no mapping). (b) Imaging result: angle-dependent reflectivity information is distorted. (c) As in (a), after mapping from k_x to p. (d) Modulus of the imaged result, obtained by adding all frequency contributions in (c). The angle-dependent reflectivity information is fully preserved.

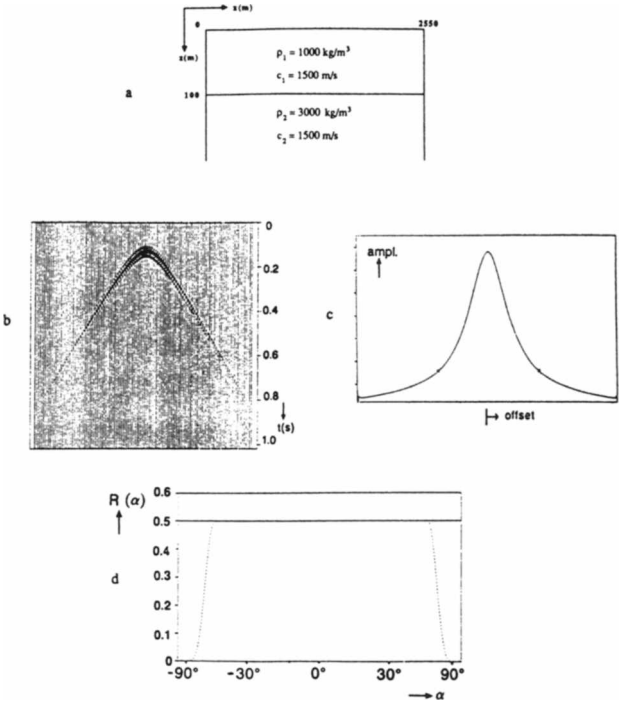

FIG. 9. Interface with density contrast only. (a) Acoustic subsurface model containing one reflection boundary. (b) Simulated seismic response from this reflection boundary (one shot record). (c) AVO result, obtained via amplitude picking along the hyperbola in (b). (d) Modulus of the angle-dependent reflection coefficient as a function of the angle of incidence (dashed line for the migration result; solid line for the theoretical result).

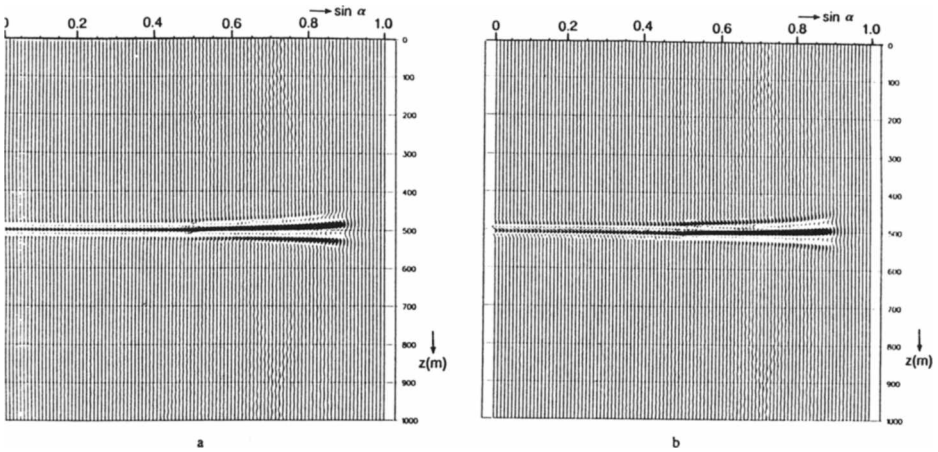

FIG. 8. Angle-dependent reflectivity image for positive angles of incidence. (a) Real part of the angle-dependent reflection coefficient as a function of depth. (b) Imaginary part of the angle-dependent reflection coefficient as a function of depth.

matic reflection function is displayed in Figure 6b. For comparison, the analytically computed angle-dependent reflection coefficient is shown in Figure 6c. Note that there is a perfect match up to a high angle of incidence far beyond the critical angle (α_{cr} = 30 degrees). It is obvious that the convolution operator of Figure 6a, compared to the delta pulse of the zero-offset reflection, contains a lot more information, namely, the total angle-dependent reflectivity characteristic. The migration result (Figures 6a and 6b) is spatially band-limited; the analytically computed result (Figure 6c) also shows the reflectivity for the evanescent wave field ($|\sin \alpha| > 1$). For comparison, the AVO result, obtained by amplitude picking along the hyperbola in Figure 5b, is depicted in Figure 6d.

In the broad-band case we repeat these computations for each frequency component in the seismic signal. Figure 7a shows the moduli of the reflection function as a function of k_x for different frequencies. The linear frequency dependence of this horizontal wavenumber can be clearly discerned. The imaging step according to equation (11) yields a distorted result in which we are not able to detect the true angle-dependent reflectivity any more (Figure 7b). However, if we first apply the mapping procedure as described by equation (13), the reflectivity information related to each angle of incidence α is preserved on lines of constant p. The mapped results are shown in Figure 7c. In the rayparameter-frequency domain we can now add all frequency contributions, according to equation (14), without losing angle dependent reflectivity information (see Figure 7d).

Note that we immediately applied the angle-dependent reflectivity imaging at the reflector depth. Normally the migration will be carried out recursively through the subsurface with small depth steps. Per lateral position we get a $p - z$ panel as is shown in Figure 8. By amplitude picking along the event, the angle-dependent reflection coefficient is obtained (Figure 7d). For this example, for both precritical reflection and for postcritical reflection, angle-dependent reflectivity can be retrieved from surface data (shown in Figure 5b) by prestack migration.

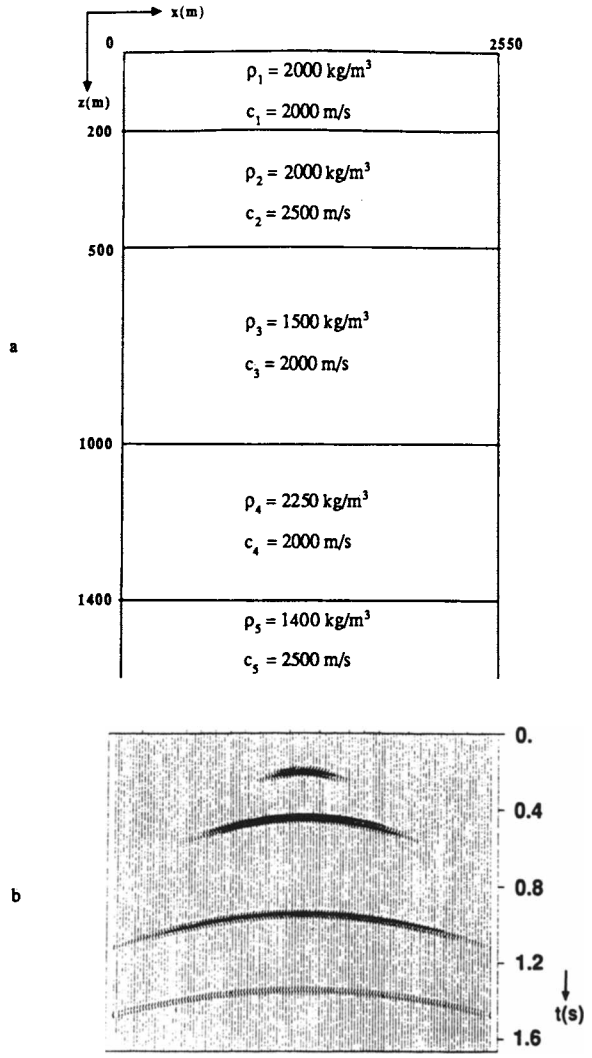

FIG. 10. (a) Subsurface model of a horizontally layered acoustic medium, containing four reflectors. (b) Simulated seismic response from the acoustic model; four reflection hyperbolas can be discerned.

ANGLE-DEPENDENT REFLECTIVITY FROM ACOUSTICALLY MODELED DATA

In this section we consider two acoustic subsurface models (de Bruin, 1988). The first model has a reflection boundary with density contrast only, and the second model has four different reflection boundaries. A split-spread CSG configuration is used with a dipole source (frequency content 10–70 Hz) and with 256 (ideal) detectors, spaced 10 m apart. The time sample interval is 4 ms. Since we are dealing with laterally invariant media, the information in one shot record is sufficient. We present only the broad-band results (after imaging) on angle-dependent reflectivity.

Density contrast

The model is shown in Figure 9a and the detected wave field in Figure 9b. The amplitude cross-section in Figure 9c exhibits the effects of the source directivity of the dipole and geometrical spreading. In Figure 9d the modulus of the *angle-independent* reflection coefficient, obtained with our prestack migration algorithm, is shown by the dashed line. The amplitude is constant at 1/2, as can be verified with equation (7). This example clearly illustrates that our method (Figure 9d) removes overburden effects which deteriorate the AVO display (Figure 9c).

Multilayered acoustic subsurface model

The configuration is depicted in Figure 10a. We first consider the noise-free situation. The $x - t$ registration at the surface is shown in Figure 10b. The results on the angle-dependent reflection coefficients, retrieved from the data set of Figure 10b by means of our prestack migration algorithm, are presented in Figure 11. The migration results are good up to critical reflection (there is no postcritical reflection information in the data of Figure 10b). For comparison, the AVO results are shown in Figure 12. From the above results we conclude that the developed imaging technique also holds for multilayered subsurface models.

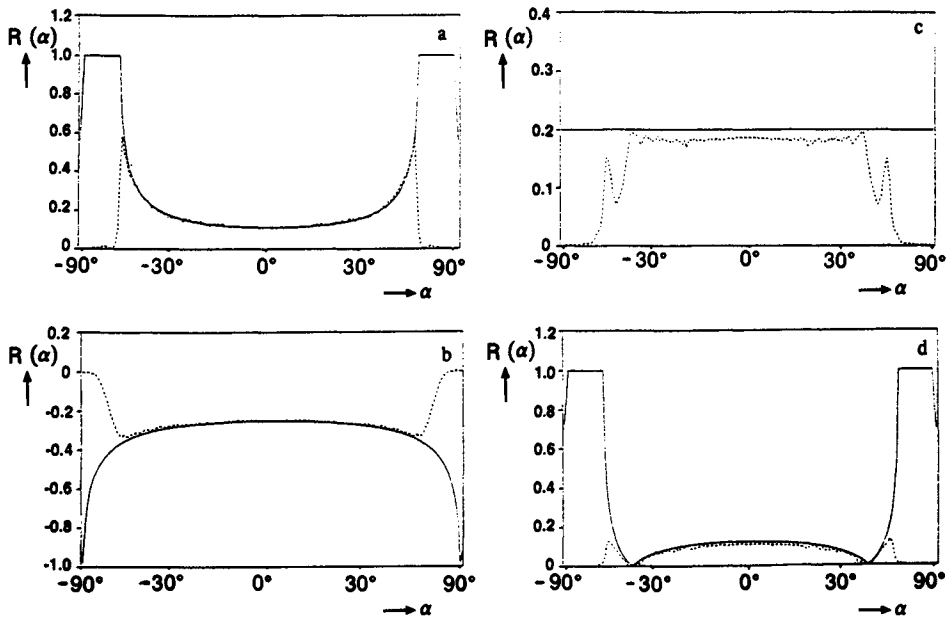

FIG. 11. Angle-dependent reflection coefficients for the model containing four reflectors (Figure 10). Migration results are displayed by the dashed lines, theoretical results by the solid lines. (a) Modulus of the angle-dependent reflection coefficient at z_1 = 200 m. (b) Real part of the angle-dependent reflection coefficient at z_2 = 500 m. (c) Modulus of the angle-independent reflection coefficient at z_3 = 1000 m. (d) Modulus of the angle-dependent reflection coefficient at z_4 = 1400 m.

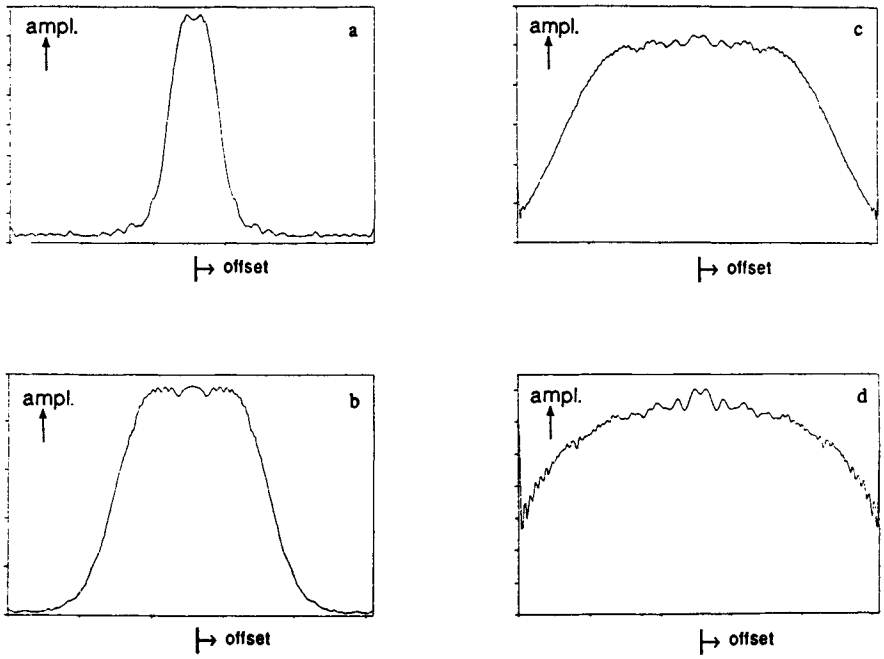

FIG. 12. Amplitude-versus-offset results for the model containing four reflectors (Figure 10). (a) First reflector at z_1 = 200 m. (b) second reflector at z_2 = 500 m. (c) third reflector at z_3 = 1000 m. (d) fourth reflector at z_4 = 1400 m.

Influence of noise

In our next example we consider the same acoustic model but noise added to the input data. The signal-to-noise ratio (SNR) is 15 dB. (The SNR is defined as the logarithm of the ratio of the maximum in the signal spectrum and the root mean square of the noise spectrum.) The noise amplitude distribution is Gaussian and the spectrum is white. The data set with this noise is shown in Figure 13. Note that the response from the deepest reflector can hardly be seen any longer.

In Figure 14 the angle-dependent reflectivity results, retrieved by prestack migration from these noisy data, are displayed. The effect of the noise can be clearly discerned from the deviations around the exact results. The trend, however, can still be determined from these results. Also compare with the noise-free results and the AVO results in Figure 15. Further it is remarkable that the angle-dependent reflectivity could also be retrieved from the fourth reflector. The results with these noisy input data are not at all disappointing, since they are obtained via (SNR improving) prestack migration.

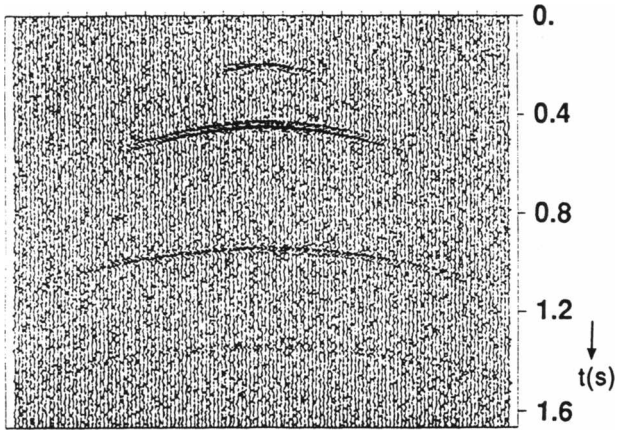

FIG. 13. The seismic response for the acoustic model, containing four reflectors (Figure 10), with noise added (SNR: 15 dB).

ANGLE-DEPENDENT REFLECTIVITY FROM ELASTICALLY MODELED DATA

The real Earth's subsurface contains solid rock layers, in which *both* compressional and shear (*S* or transversal) waves may exist. The acoustic approximation has proven to be acceptable for data without large offsets. Wave conversions ($P \rightarrow S$; $S \rightarrow P$) can be neglected for small angles of incidence. In our research we are also interested in wide-angle reflectivity information contained by large-offset data; therefore, the effect of wave conversions cannot be neglected any longer. Hence, retrieving the *elastic* angle-dependent reflectivity characteristic is more refined than the *acoustic* one.

Full elastic subsurface model

We consider the horizontally layered elastic subsurface model, shown in Figure 16. This model consists of three macro layers with different elastic parameters and a target zone below z = 1450 m, consisting of four thin layers. The model is bounded by a free surface at z = 0 m and by a homogeneous half-space below the target zone. For this model we simulated a multicomponent shot record. We

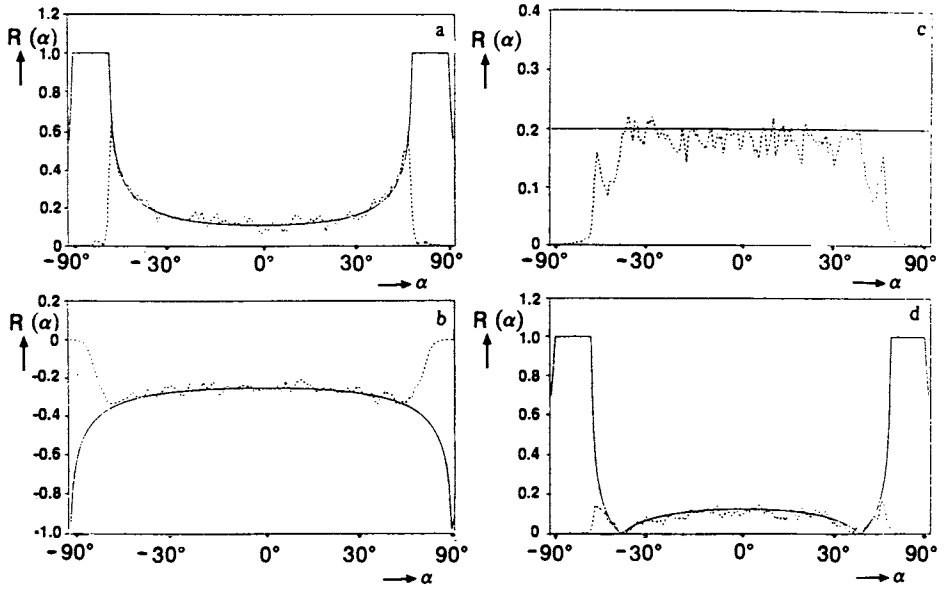

FIG. 14. Angle-dependent reflection coefficients from the noisy data set in Figure 13. Migration results are displayed by the dashed lines, theoretical results by the solid lines. (a) Modulus of the angle-dependent reflection coefficient at z_1 = 200 m. (b) Real part of the angle-dependent reflection coefficient at z_2 = 500 m. (c) Modulus of the angle-independent reflection coefficient at z_3 = 1000 m. (d) Modulus of the angle-dependent reflection coefficient at z_4 = 1400 m.

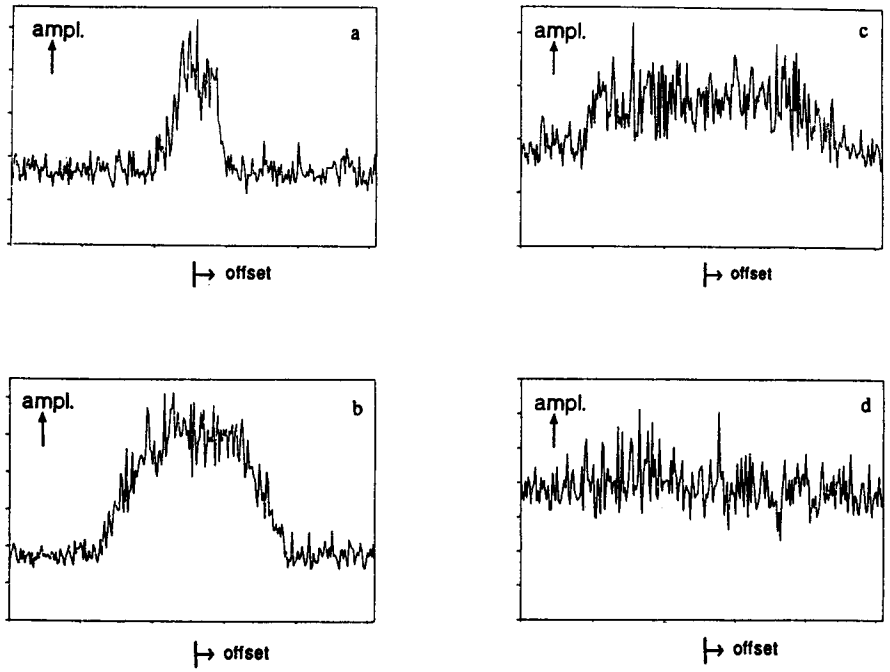

FIG. 15. Amplitude-versus-offset results from the noisy data set in Figure 13. (a) First reflector at z_1 = 200 m. (b) second reflector at z_2 = 500 m. (c) third reflector at z_3 = 1000 m. (d) fourth reflector at z_4 = 1400 m.

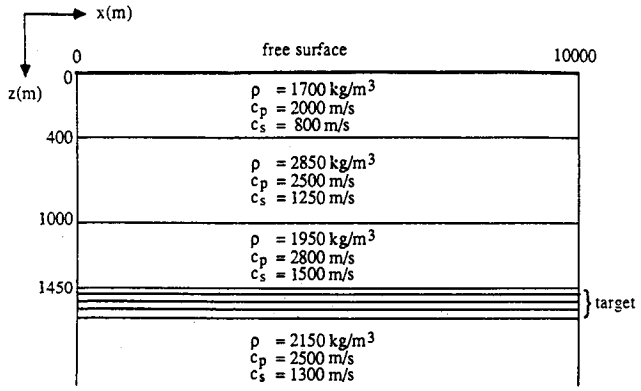

FIG. 16. Horizontally layered elastic model bounded by a free surface at z = 0 m.

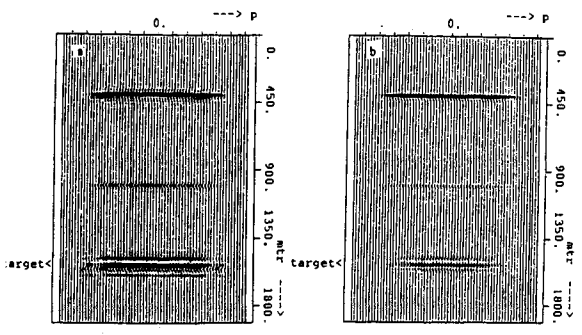

FIG. 17. Angle-dependent reflectivity images (real part), obtained by prestack migration. (a) $R_{P\text{-}P}(p, z)$ section. (b) $R_{SV\text{-}SV}(p, z)$ section.

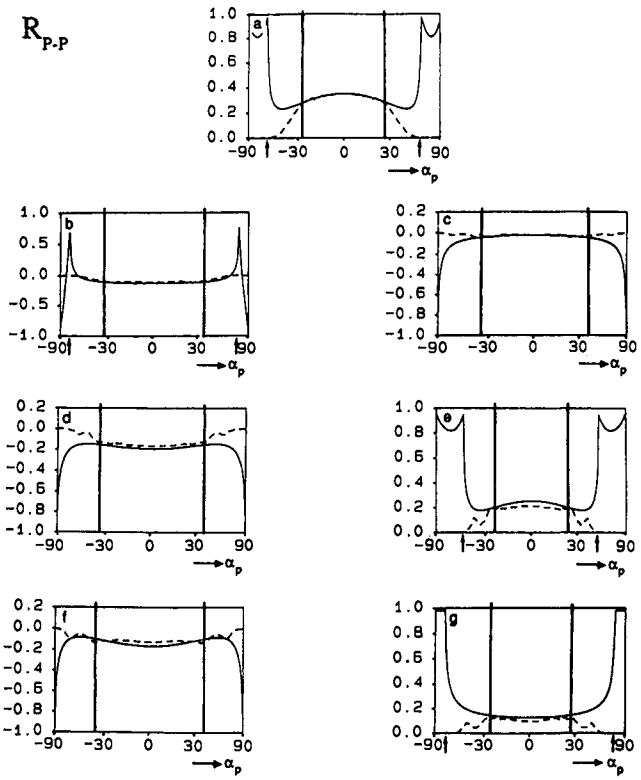

FIG. 18. Angle-dependent reflection coefficient $R_{P\text{-}P}(\alpha_P)$, obtained from Figure 17a (dotted lines) and computed analytically (solid lines). Figures 18a–18g correspond to reflector numbers 1, 2, 3, 4, 5, 6, 7, respectively. The arrows indicate the first critical angle for an incident P-wave. The vertical bars indicate the spatial bandwidth of the input data.

restrict ourselves to determining $R_{P\text{-}P}$ and $R_{S\text{-}S}$. The results on angle-dependent reflectivity in the p-z domain by means of prestack migration are presented in Figure 17. The ray parameter p is defined as

$$p = \frac{\sin \alpha_P(z)}{c_P(z)} = \frac{\sin \alpha_S(z)}{c_S(z)},$$

where $\alpha_P(z)$ and $\alpha_S(z)$ are the depth-dependent propagation angles of P- and SV-waves, respectively, and where $c_P(z)$ and $c_S(z)$ are the depth-dependent P- and SV-wave propagation velocities, respectively. For this horizontally layered model the ray parameter p is independent of depth (Snell's law). Figures 17a and 17b represent the reflectivity sections $R_{P\text{-}P}(p, z)$ and $R_{SV\text{-}SV}(p, z)$, obtained by migration from the true P-P and true SV-SV data, after applying two preprocessing steps (decomposition and multiple elimination, see Figure 1).

From the results in Figures 17a and 17b we retrieved angle-dependent reflection coefficients at the various reflector depth levels by amplitude picking. The migration results are shown by the dashed lines in Figures 18 (P-P) and 19 (SV-SV), respectively, where they are compared with the exact reflection coefficients (solid lines). Note the good match up to angles approaching critical reflection (postcritical reflections were not present in the input data). We emphasize that the different reflectivity sections were obtained by fully *independently* migrating the P-P and SV-SV responses. So the developed imaging technique has performed quite well for this full elastic subsurface model also.

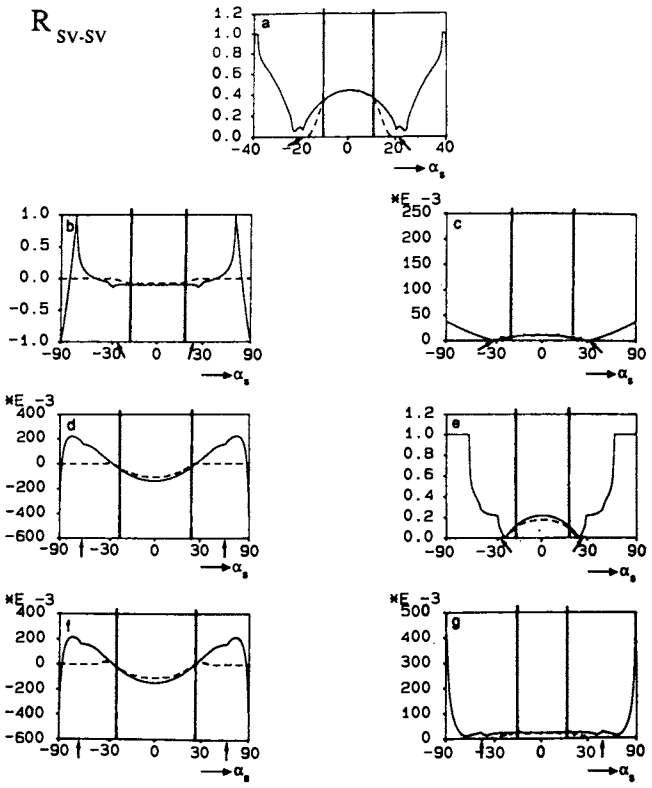

FIG. 19. Angle-dependent reflection coefficient $R_{SV\text{-}SV}(\alpha_S)$, obtained from Figure 17b (dotted lines) and computed analytically (solid lines). Figures 19a–19g correspond to reflector numbers 1, 2, 3, 4, 5, 6, 7, respectively. The arrows indicate the first critical angle for an incident SV-wave. The vertical bars indicate the spatial bandwidth of the input data.

CONCLUSIONS

Multiexperiment, multioffset seismic data contain information on the angle-dependent properties of the reflectivity of the subsurface. Moreover, *multicomponent* seismic data contain information on the angle-dependent behavior of the reflectivity for different wave types. In spite of this wealth of information in the seismic data, current seismic migration schemes aim at nothing more than representing the Earth's subsurface by one average reflection coefficient per depth point. Berkhout and Wapenaar (1988) have proposed a new step-wise seismic processing scheme which takes full advantage of the angle-dependent reflectivity information present in the seismic data (Figure 1). The central step in this scheme is prestack migration of well-separated P-P, P-S, S-P, and S-S responses, aiming at determining the angle-dependent P-P, P-S, S-P, and S-S reflectivities per depth point.

We have discussed the principle of imaging angle-dependent reflectivity from surface data by prestack migration. We have shown that it is possible to retrieve the angle-dependent reflectivity $R_{P\text{-}P}(x, z; \alpha)$ and $R_{SV\text{-}SV}(x, z; \alpha)$. Once these functions are found, it is in principle possible to determine the detailed density and P- and S-wave velocities in a subsequent inversion step. With some simple examples we have demonstrated the validity of our approach for 1-D media. Both in the acoustic and the elastic cases, the results are very promising. We expect that imaging angle-dependent reflectivity is going to play an important role in AVO techniques.

REFERENCES

Berkhout, A. J., 1985, Seismic migration: Imaging of acoustic energy by wave field extrapolation. A. Theoretical aspects: Elsevier Science Publ. Co., Inc.

Berkhout, A. J., and Wapenaar, C. P. A., 1988, Delft philosophy on inversion of elastic data: Presented at the 58th Ann. Internat. Mtg., Soc. Expl. Geophys., Expanded Abstracts, 831–833.

Claerbout, J. F., 1976, Fundamentals of geophysical data processing: McGraw-Hill Book Co.

Cox, H. L. H., Kinneging, N. A., Wapenaar, C. P. A., and Berkhout, A. J., 1989, Efficient macro-model estimation: Presented at the 59th Ann. Internat. Mtg., Soc. Expl. Geophys., Expanded Abstracts, 1229–1232.

de Bruin, C. G. M., 1988, Angle-dependent reflectivity by shot record migration: M.Sc. Thesis, Delft University of Technology; Presented at the 58th Ann. Internat. Mtg., Soc. Expl. Geophys., Expanded Abstracts, 1093–1096.

de Haas, J. C. and Berkhout, A. J., 1989, Practical approach to nonlinear inversion of amplitude-versus-offset information: Presented at the 59th Ann. Internat. Mtg., Soc. Expl. Geophys., Expanded Abstracts, 839–842.

Herrmann, P., Wapenaar, C. P. A., and Berkhout, A. J., 1989, Seismic preprocessing in terms of wave field decomposition at the surface: Presented at the 59th Ann. Internat. Mtg., Soc. Expl. Geophys., Expanded Abstracts, 1312–1315.

Kinneging, N. A., Budejicky, V., Wapenaar, C. P. A., and Berkhout, A. J., 1989, Efficient 2-D and 3-D shot record redatuming: Geophys. Prosp., **37**, 493–530.

Lörtzer, G. J. M., and Berkhout, A. J., Lithologic inversion of seismic information with result analysis: Presented at the 59th Ann. Internat. Mtg., Soc. Expl. Geophys., Expanded Abstracts, 867–870.

Resnick, J. R., Ng, P., and Larner, K., 1987, Amplitude Versus Offset Analysis in the Presence of Dip: Presented at the 57th Ann. Internat. Mtg., Soc. Expl. Geophys., Expanded Abstracts, 617–620.

Tarantola, A., 1986, A strategy for nonlinear elastic inversion of seismic reflection data: Geophysics, **51**, 1893–1903.

Verschuur, D. J., Berkhout, A. J., and Wapenaar, C. P. A., 1989, Wavelet Estimation by Prestack Multiple Elimination: Presented at the 59th Ann. Internat. Mtg., Soc. Expl. Geophys., Expanded Abstracts, 1129–1132.

Wapenaar, C. P. A., and Berkhout, A. J., 1989, Elastic wave field extrapolation. Redatuming of single- and multi-component seismic data: Elsevier Science Publ. Co., Inc.

Wapenaar, C. P. A., Herrmann, P., Verschuur, D. J., and Berkhout, A. J., 1990, Decomposition of multi-component seismic data into primary *P* and *S* wave responses: accepted for publication in Geophys. Prosp.

DOI:10.1190/1.1442938